Ground and doubly excited states of two-dimensional D^- centers

W. Y. Ruan*
Department of Applied Physics, South China University of Technology, Guangzhou 510641, People's Republic of China

K. S. Chan
Department of Physics and Materials Science, City University of Hong Kong, Hong Kong, People's Republic of China

E. Y. B. Pun
Department of Electronic Engineering, City University of Hong Kong, Hong Kong, People's Republic of China
(Received 14 September 2000; revised manuscript received 5 December 2000; published 19 April 2001)

Using hyperspherical coordinates and assuming the quasiseparability of the hyperradius R from the angular variables Ω in the wave functions, we obtain the low-lying adiabatic channel potentials $U_\mu(R)$ for the two-dimensional D^- centers. In the large-R limit, these potential curves converge to the thresholds of the energy levels of the neutral donor. The energy eigenstates supported by these potentials are calculated. The correlation patterns in these channels and the effect of symmetry are investigated.

DOI: 10.1103/PhysRevB.63.205204 PACS number(s): 78.66.Fd, 71.35.−y, 73.21.−b, 78.20.Ls

I. INTRODUCTION

A two-dimensional D^- center consists of a fixed positive ion and two electrons, all confined to the x-y plane. Its existence was first observed by Huant, Najda, and Etienne in selectively doped GaAs-$Ga_{1-x}Al_xAs$ multiple-quantum-well structures,[1] where the binding energies were measured as a function of the external magnetic field. This has stimulated numerous theoretical investigations of the system. Using the effective-mass model and the diffusion quantum Monte Carlo approach,[2] Pang and Louie calculated the ground-state energy of the D^- center in a magnetic field, and found good agreement between theory and experiments. Exact solutions for a D^- center in a strong magnetic field have been obtained independently by Larsen and McCann,[3] Dzyubenko,[4] and MacDonald.[5] The effects of electron-phonon interaction and of the finite width of the quantum well have been studied by Shi, Peeters, and Devreese.[6] The effect of position deviation of the donor from the well center has been considered in a number of recent studies.[7–10] Two well-established facts from all these studies are that the electron correlation is very important in this small system and that the reduced dimensionality considerably enhances the binding energies.

The aim of this paper is not to improve the previous calculations to bring theory closer to experiment but to provide a comprehensive understanding of the low-lying spectrum and the associated patterns of correlation of this simplest Coulomb system with electron-electron interaction. In particular, as will be shown in the following, the reduced dimensionality not only enhances the binding but also results in extra symmetries which do not have counterparts in three dimensions, and thus enriches the patterns of correlation. For this purpose, in this paper we use the adiabatic hyperspherical method to make a systematic study of the low-lying doubly excited states of the D^- center, where the correlation is even stronger than that in the ground state. The method of expanding the trial wave function in terms of hyperspherical harmonics[11] suffers from extremely slow convergence for the doubly excited states. The adiabatic hyperspherical method was first introduced to the study of correlation effects in Coulombic systems by Macek in 1968,[12] and has since developed into a powerful tool for understanding the electron correlations in the doubly excited states in the spectra of He and H^-.[13] A principal advantage of the method is the reduction of a multidimensional problem to a one-dimensional problem with a set of effective potentials. These potentials provide qualitative and quantitative information about the dynamics of the system. More importantly, the method automatically projects the quantum spectrum into vibrational bands in R, and thus gives a useful and convenient classification scheme.

Mathematically, the adiabatic hyperspherical method is similar to the Born-Oppenheimer approximation in diatomic molecules (note that the mass-weighted hyperradius coincides with the internuclear separation for diatomic systems in the heavy-nucleus limit). Hence its validity is not obvious for D^- centers and the like. In the Born-Oppenheimer approximation, the wave functions of the molecules are expressed as the products of electronic and vibrational nuclear wave functions. This quasiseparability is conventionally justified by the argument that the mass m_e of the electron is much less than the mass M of the nucleus and thus the vibrational motion of the nuclei is adiabatic in comparison with the faster electronic motion. However, this argument is not substantially supported by the actual magnitude of the nonadiabatic correction.[14] The correction is proportional to $(m_e/M)^{1/4} \sim \frac{1}{6}$, while precise calculations[15,16] for the low-lying states of H_2^+ and H_2 show that the nonadiabatic effect is only of the order 10^{-5}. Therefore, there are other underlying dynamical factors responsible for the validity of the adiabatic approximation in molecular physics. As has been pointed out by several authors,[17–19] the slow variation of the strength of the Coulombic interactions with R, and the fact that the kinetic energy associated with the motion in R is much smaller than that associated with Ω due to the limited ranges of the angular variables, are responsible for the adiabaticity. There has been much work demonstrating that the eigenenergies and eigenfunctions of the doubly excited states calculated in the

adiabatic hyperspherical approximation agree quite well with the results of other theoretical calculations and with experiments.[12,20–23] There has also been some work demonstrating that the validity of the approximation weakly depends on the masses of the particles.[21,24,25] In this paper, we further assume that the reduced dimensionality should not influence the validity of the approximation.

In the following section, details of our numerical method are described. The numerical results are presented in Sec. III. Some concluding remarks are presented in Sec. IV.

II. FORMALISM

For two electrons bound to a positively charged donor ion in an ideal two-dimensional quantum well, the Schrödinger equation reads

$$\left[-\frac{1}{2}\nabla_{\mathbf{r}_1}^2-\frac{1}{2}\nabla_{\mathbf{r}_2}^2-\frac{1}{r_1}-\frac{1}{r_2}+\frac{1}{r_{12}}\right]\Psi(\mathbf{r}_1,\mathbf{r}_2)=E\Psi(\mathbf{r}_1,\mathbf{r}_2), \tag{1}$$

where $\mathbf{r}_1$ and $\mathbf{r}_2$ measure the positions of the two electrons from the donor ion. Atomic units (a.u.) are used throughout this paper.

With $\mathbf{r}_1$ and $\mathbf{r}_2$, the simplest hyperspherical coordinates are obtained by substituting r_1 and r_2 with

$$R=(r_1^2+r_2^2)^{1/2}, \quad \alpha=\tan^{-1}(r_2/r_1). \tag{2}$$

The hyperradius R measures the size of the system, while the hyperangle α represents the radial correlation of the motion of two electrons. Thus the two vectors $\mathbf{r}_1$ and $\mathbf{r}_2$ are now replaced by four coordinates (R,Ω), where $\Omega\equiv(\alpha,\theta_1,\theta_2)$ collectively denotes the three angles, with θ_i being the polar angle of electron i.

In hyperspherical coordinates, the Schrödinger equation (1) can be expressed as

$$\left\{-\frac{1}{2}\left[\frac{\partial^2}{\partial R^2}+\frac{3}{R}\frac{\partial}{\partial R}-\frac{\Lambda^2(\Omega)}{R^2}\right]+\frac{C(\Omega)}{R}\right\}\Psi(R,\Omega) =E\Psi(R,\Omega), \tag{3}$$

where

$$\Lambda^2(\Omega)=-\frac{\partial^2}{\partial\alpha^2}-\left(\frac{\cos\alpha}{\sin\alpha}-\frac{\sin\alpha}{\cos\alpha}\right)\frac{\partial}{\partial\alpha}+\frac{\hat{L}_1^2}{\cos^2\alpha}+\frac{\hat{L}_2^2}{\sin^2\alpha} \tag{4}$$

is the grand orbital operator, and

$$C(\Omega)=-\frac{1}{\cos\alpha}-\frac{1}{\sin\alpha}+\frac{1}{\sqrt{1-\sin(2\alpha)\cos\theta_{12}}}, \tag{5}$$

where $\theta_{12}=\theta_2-\theta_1$. Equation (3) is similar in structure to the Schrödinger equation of a hydrogen atom in four space dimensions, with $-C(\Omega)$ as the effective nuclear charge. Figure 1 is a three-dimensional plot of the potential surface $C(\Omega)$ on the plane (α,θ_{12}) in the ranges $0\leqslant\alpha\leqslant90°$ and $0\leqslant\theta_{12}\leqslant360°$. In the limit $\alpha\sim0$ or $\alpha\sim90°$, a configuration where one electron is much closer to the ion than the other, the potential surface has a sharp drop caused by the electron-ion attraction. This configuration is expected to be important in the ground state in which the total energy of the system is minimized. In the situation where $r_1\approx r_2$, which corresponds to $\alpha\approx45°$, the potential surface depends critically on θ_{12}. When $\alpha=45°$ and $\theta_{12}\approx0$ or 360°, the two electrons lie close to each other in the configuration space, where a large electron-electron repulsion is expected. In Fig. 1 this repulsion appears as two spikes at $(\alpha,\theta_{12})=(45°,0)$ and $(45°,360°)$, respectively. $(\alpha,\theta_{12})=(45°,180°)$ is a saddle point, over a large area around which the potential surface is very flat. The existence of a saddle point is important for the doubly excited states to be discussed in the following.

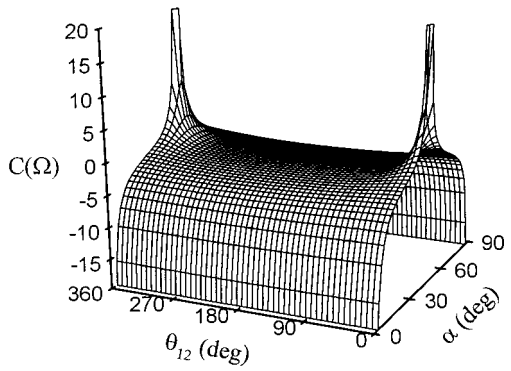

FIG. 1. Three-dimensional plot of $C(\alpha,\theta_{12})$ in hyperspherical coordinates.

A. The adiabatic-channel expansion method

Following Macek's prescription,[12] we expand the trial wave function in terms of the channel functions

$$\Psi(R,\Omega)=R^{-3/2}\sum_{\mu}F_{\mu}(R)\Phi_{\mu}(R,\Omega), \tag{6}$$

where μ is the channel index. The channel functions Φ_{μ} are eigenfunctions of the eigenequation

$$\hat{U}\Phi_{\mu}(R,\Omega)=U_{\mu}(R)\Phi_{\mu}(R,\Omega), \tag{7}$$

where

$$\hat{U}=\frac{1}{2}\frac{\Lambda^2+3/4}{R^2}+\frac{C(\Omega)}{R}. \tag{8}$$

Equation (7) is equivalent to solving the Schrödinger equation at constant values of R, neglecting the derivatives with respect to R. Therefore, the channel functions, parametrically depending on R, represent standing waves on the potential surface $C(\Omega)$ shown in Fig. 1. Since all the channel functions form a complete set, the expansion in Eq. (6) contains no approximation.

Substituting Eqs. (6) into (3), multiplying Eq. (3) by $[\Phi_{\mu}(R,\Omega)]^*$ from the left, integrating over the angular variables, and making use of Eq. (7), we obtain a set of coupled equations for determining $\{F_{\mu}(R)\}$,

$$-\frac{1}{2}\frac{d^2F_\mu(R)}{dR^2}+U_\mu(R)F_\mu(R)+\sum_{\mu'} W_{\mu,\mu'}(R)F_{\mu'}(R) = EF_\mu(R), \tag{9}$$

where

$$W_{\mu,\mu'}(R)=-\frac{1}{2}\left\langle \phi_\mu(R,\Omega)\left|\frac{\partial^2}{\partial R^2}\right|\phi_{\mu'}(R,\Omega)\right\rangle - \left\langle \phi_\mu(R,\Omega)\left|\frac{\partial}{\partial R}\right|\phi_{\mu'}(R,\Omega)\right\rangle\frac{\partial}{\partial R} \tag{10}$$

are the coupling matrix elements.

B. The channel functions and channel potentials

As a first step of the approach, our task is to find out the eigensolutions of Eq. (7). Generally speaking, exact analytical solutions of Eq. (7) that are valid at any R value do not exist. However, its eigensolutions in the limits of $R=0$ and $R\to\infty$ are readily obtained. From Eq. (8), we note that when $R\sim 0$ the electrostatic potential energy $C(\Omega)/R$ becomes negligible compared to the kinetic energy $(\Lambda^2+3/4)/(2R^2)$. The channel functions $\Phi_\mu(R)$ approach the eigenfunctions of Λ^2,

$$\Phi_\mu(R,\Omega)\to Y_{\{\nu l_1 l_2\}}(\Omega)=N_\nu^{l_1 l_2}P_\nu^{l_1 l_2}(\alpha)e^{il_1\theta_1}e^{il_2\theta_2}, \tag{11}$$

and the channel potential is

$$U_\mu(R)\to\frac{1}{2}\frac{\lambda(\lambda+2)+3/4}{R^2}, \tag{12}$$

where $\lambda=2\nu+|l_1|+|l_2|$. In Eq. (11), $N_\nu^{l_1 l_2}$ is the normalization constant, and $P_\nu^{l_1 l_2}$ is a Jacobi polynomial, given by

$$N_\nu^{l_1 l_2}=\left(\frac{2(2\nu+|l_1|+|l_2|+1)\nu!(\nu+|l_1|+|l_2|)!}{4\pi^2(\nu+|l_1|)!(\nu+|l_2|)!}\right)^{1/2} \tag{13}$$

and

$$P_\nu^{l_1 l_2}(\alpha)=\sum_{k=0}^{\nu}(-)^{\nu-k}\binom{\nu+|l_2|}{k}\binom{\nu+|l_1|}{\nu-k} \times(\cos\alpha)^{2k+|l_1|}(\sin\alpha)^{2(\nu-k)+|l_2|}. \tag{14}$$

In the limit of $R\to\infty$ and $\alpha\to\pi/2$ such that $r_1=R\cos\alpha$ remains finite and $r_2=R\sin\alpha\approx R$, the operator $\hat{U}$ approaches the hydrogenic Hamiltonian $\hat{H}(\mathbf{r}_1)$, i.e.,

$$\hat{U}=\hat{H}(\mathbf{r}_1)+\frac{\hat{L}_2^2}{R^2}+\frac{r_1\cos\theta_{12}}{R^2}+O\left\{\frac{1}{R^3}\right\}, \tag{15}$$

and $\Phi_\mu(R,\Omega)$ and $U_\mu(R)$ are

$$\Phi_\mu(R,\Omega)\to\phi_{nl_1}(\mathbf{r}_1)e^{il_2\theta_2}, \tag{16}$$

$$U_\mu(R)\to\epsilon_n=-\frac{1}{2}\frac{1}{(n+1/2)^2}. \tag{17}$$

In Eq. (16), ϕ_{nl} are two-dimensional hydrogenic wave functions,

$$\phi_{nl}(\mathbf{r})=\left[\frac{(n-|l|)!}{\pi(n+1/2)^3(n+|l|)!}\right]^{1/2}\rho^{|l|}L_{n-|l|}^{(2|l|)}(\rho)e^{-\rho/2}e^{il\theta}, \tag{18}$$

where $\rho=2r/(n+1/2)$. n is the principal quantum number, $n=0,1,2,\ldots$; ϵ_n is the corresponding eigenenergy; $L_n^{(\alpha)}$ are Laguerre polynomials. The right-hand side of Eq. (16) corresponds to the fact that electron 1 is in its nl_1 orbital and electron 2 has an angular momentum l_2. The asymptotic results as $R\to\infty$ and $\alpha\to 0$ can be obtained by exchanging the electron coordinates $(r_1,\theta_1)\leftrightarrow(r_2,\theta_2)$ in Eqs. (15) and (16). Notice that the energy level ϵ_n is $(2n+1)$-fold degenerate. The actual channel functions will be the superpositions of $(2n+1)$ hydrogenic wave functions in the large-R limit. The third term on the right-hand side of Eq. (15) represents the dipole interaction between the neutral donor and the outer electron 2, which is expected to lift the degeneracy in ranges of finite R.

In the hydrogenic wave functions $\phi_{nl}(\rho)$, when ρ is replaced by hyperspherical coordinates, the polynomial parts $\rho^{|l|}L_{n-|l|}^{(2|l|)}(\rho)$ are readily reexpressed as the superposition of a finite set of hyperspherical harmonics, while the exponentially decaying factor $e^{-\rho/2}$, which changes drastically with α when R is large, cannot be reproduced by a small set of hyperspherical harmonics. Due to this fact, any calculations with hyperspherical harmonics as basis functions alone are inaccurate. Taking into account this fact and the exchange symmetry, we choose a model space spanned by the following nonorthogonal functions:

$$|n\nu l_1 l_2\pm\rangle^e=\{P_\nu^{l_1 l_2}(\alpha)e^{-R\cos\alpha/(n+1/2)} \pm P_\nu^{l_2 l_1}(\alpha)e^{-R\sin\alpha/(n+1/2)}\} \times\cos\left[\frac{l_2-l_1}{2}\theta_{12}\right]e^{iL\Theta} \tag{19}$$

and

$$|n\nu l_1 l_2\pm\rangle^o=\{P_\nu^{l_1 l_2}(\alpha)e^{-R\cos\alpha/(n+1/2)} \pm P_\nu^{l_2 l_1}(\alpha)e^{-R\sin\alpha/(n+1/2)}\} \times\sin\left[\frac{l_2-l_1}{2}\theta_{12}\right]e^{iL\Theta} \tag{20}$$

to diagonalize the operator $\hat{U}$ to obtain the channel functions and channel potentials at each intermediate R value. In Eqs. (19) and (20), $L=l_1+l_2$ and $\Theta=(\theta_1+\theta_2)/2$. The superscript ''$e$'' indicates that the functions are even about θ_{12}, while the superscript ''o'' indicates that the functions are odd about θ_{12}. Throughout this paper, we do not write out the spin function explicitly. It is sufficient to remember that the spatially symmetric wave functions (e.g., $|n\nu l_1 l_2+\rangle^e$ and

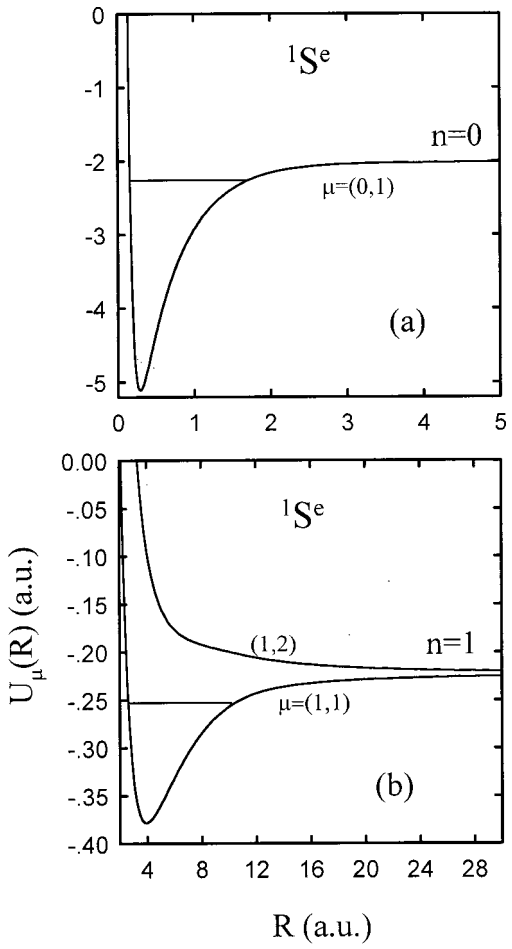

FIG. 2. Potential curves for $^1S^e$ channels converging to the ϵ_n limit: $n=$(a) 0, (b) 1. The horizontal lines mark the bound states supported by the potentials.

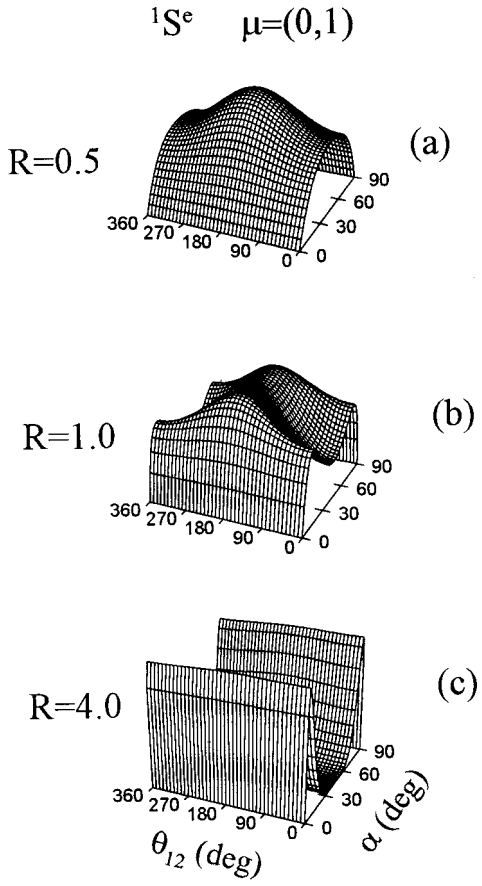

FIG. 3. Three-dimensional surface charge-density $\rho_s(R,\alpha,\theta_{12})$ plots for the $\mu=(0,1)$ channel of symmetry $^1S^e$.

$|n\nu l_1 l_2-\rangle^o$) describe the spin-singlet states, while the spatially antisymmetric wave functions (e.g., $|n\nu l_1 l_2-\rangle^e$ and $|n\nu l_1 l_2+\rangle^o$) describe the spin-triplet states.

From the structures of these basis functions, we mention the following properties. (a) Since $\hat{U}$ is an even function of θ_{12}, the hybridization of the basis set $\{|n\nu l_1 l_2\pm\rangle^e\}$ with set $\{|n\nu l_1 l_2\pm\rangle^o\}$ will never occur. Hence ''*e*'' and ''*o*'' are good quantum numbers for the system. They can be used to label an eigenstate. Here we would like to point out that, unlike in a three-dimensional system, the parity, now given by $(-1)^L$, is not useful in labeling a state. (b) In the states represented by $|n\nu l_1 l_2-\rangle^e$ or $|n\nu l_1 l_2-\rangle^o$, $\alpha=45°$ is a nodal line. It prohibits the two electrons from penetrating close to the donor ion simultaneously and induces an energetic motion across the ridge in Fig. 1. This implies that the radial motions of the two electrons must be out of step. In the states represented by $|n\nu l_1 l_2+\rangle^e$ or $|n\nu l_1 l_2+\rangle^o$, $\alpha=45°$ is an antinodal line. The radial motions of the two electrons are in step. (c) In the states represented by basis functions $|n\nu l_1 l_2 \pm\rangle^e$ with an odd value of L or in states represented by $|n\nu l_1 l_2\pm\rangle^o$ with an even value of L, $\theta_{12}=180°$ is a nodal line. It prohibits the two electrons from remaining on the opposite sides of the donor ion. A swing motion along the ridge of Fig. 1 is expected in these states. The nodal lines we discuss here arise from symmetries. They appear at exactly the same positions in any systems with the same symmetries. They will be called inherent nodal lines hereafter. It will soon be clear that these nodal lines primarily determine the correlation pattern and the energy level of a channel.

C. The adiabatic approximation

From Eq. (8), we note that the relative magnitude of the kinetic energy $(\Lambda^2+3/4)/(2R^2)$ and the electrostatic potential energy $C(\Omega)/R$ scales linearly with R. This slow variation in relative magnitude of the two energy terms is characteristic of Coulomb interactions. The adiabatic approximation in this context assumes that the channel functions $\Phi_\mu(R,\Omega)$ show only a slow variation with respect to R; that is, to the first order of approximation, we can neglect the channel couplings given by Eq. (10). In this paper, unless stated, we confine ourselves to this approximation. The wave function then factorizes according to

$$\Psi_\mu(R,\Omega)=F_\mu(R)\Phi_\mu(R,\Omega). \tag{21}$$

All information about particle correlation is contained in the channel functions $\Phi_\mu(R,\Omega)$. The radial wave functions $F_\mu(R)$ and the eigenenergies can be obtained by solving the decoupled equations

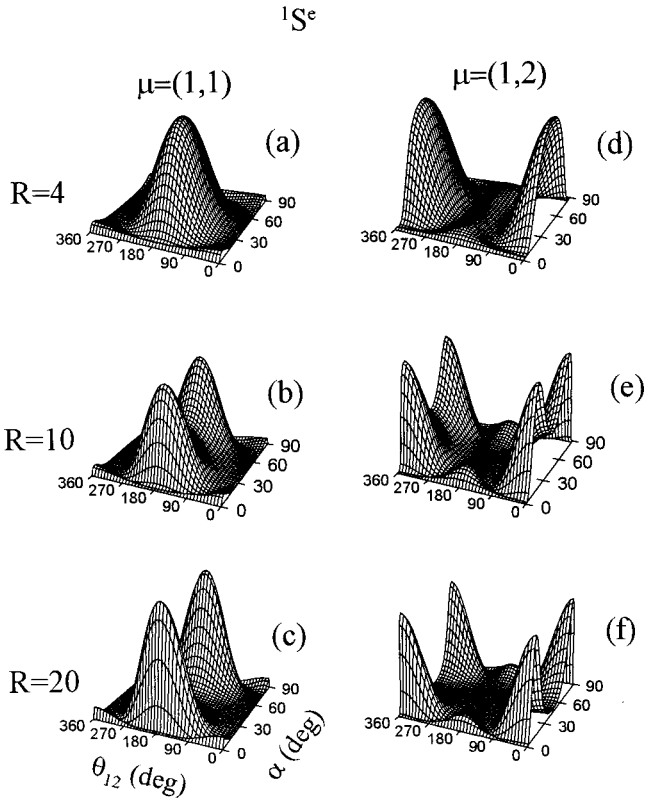

FIG. 4. Three-dimensional surface charge-density $\rho_s(R,\alpha,\theta_{12})$ plots for the $\mu=(1,1)$ and (1,2) channels of symmetry $^1S^e$.

$$-\frac{1}{2}\frac{d^2F_\mu(R)}{dR^2}+U_\mu(R)F_\mu(R)=EF_\mu(R). \tag{22}$$

The channel potentials $U_\mu(R)$ then have the physical meaning of potentials that control the motion along the coordinate R. With a channel potential $U_\mu(R)$, by solving Eq. (22) we generally obtain a series of eigenstates with their eigenenergies converging to ϵ_n, the threshold of $U_\mu(R)$. For a different $U_\mu(R)$, we obtain a different series of eigenstates. States within a series have similar correlation patterns.

III. NUMERICAL RESULTS

In this section, to avoid tediousness, we limit our numerical analysis to the $L=0$ states with various symmetries. Then the basis functions are simplified to

$$|n\nu l\pm\rangle^e=[e^{-R\cos\alpha/(n+1/2)} \pm e^{-R\sin\alpha/(n+1/2)}]P_\nu^{ll}(\alpha)\cos(l\theta_{12}) \tag{23}$$

and

$$|n\nu l\pm\rangle^o=[e^{-R\cos\alpha/(n+1/2)} \pm e^{-R\sin\alpha/(n+1/2)}]P_\nu^{ll}(\alpha)\sin(l\theta_{12}). \tag{24}$$

After obtaining the channel potentials and channel functions, to understand the particle correlation, from the normalization condition of the channel functions,

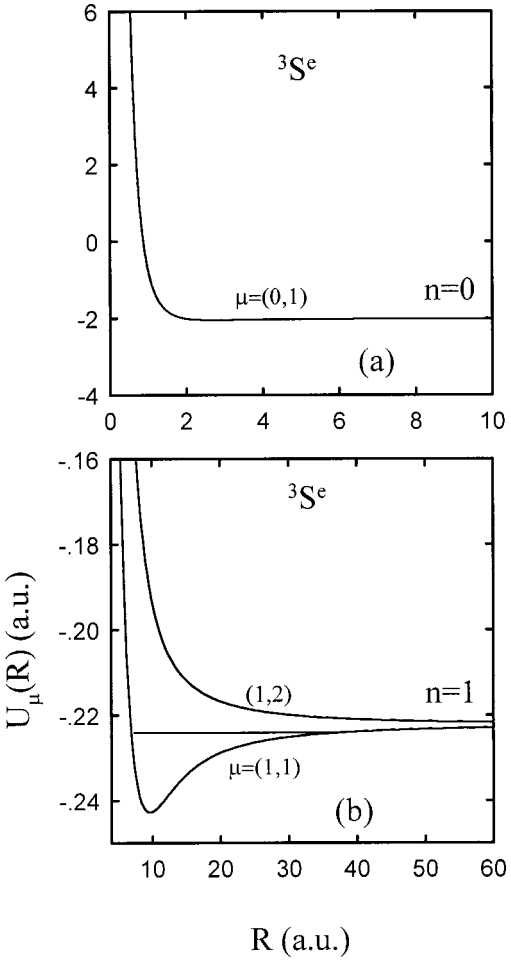

FIG. 5. Potential curves for $^3S^e$ channels converging to the ϵ_n limit: $n=$(a) 0, (b) 1. The horizontal line marks the bound states supported by the potential.

$$\int |\Phi_\mu(R,\Omega)|^2\sin\alpha\cos\alpha\,d\alpha\,d\theta_{12}d\Theta=1, \tag{25}$$

we define the surface charge density as

$$\rho_s(R,\alpha,\theta_{12})=|\Phi_\mu(R,\Omega)|^2\sin\alpha\cos\alpha. \tag{26}$$

The α dependence of ρ_s is defined as the radial correlation; the θ_{12} dependence of ρ_s is defined as the angular correlation.

A. The $^1S^e$ channels

The channel functions in the $^1S^e$ symmetry can be expressed as superpositions of the basis functions $|n\nu l+\rangle^e$. They are the channels with no inherent nodal lines. Hence, among the channels with various symmetries, they are expected to be lowest in energy. Figure 2 presents the potential curves $U_\mu(R)$ that converge to the thresholds ϵ_0 and ϵ_1, where a symbol $\mu=(n,j)$ has been used to label the jth channel converging to the nth excited state of the neutral donor.

Figure 2(a) is the potential curve for the ground channel of the $^1S^e$ symmetry, which exhibits an attractive well in the

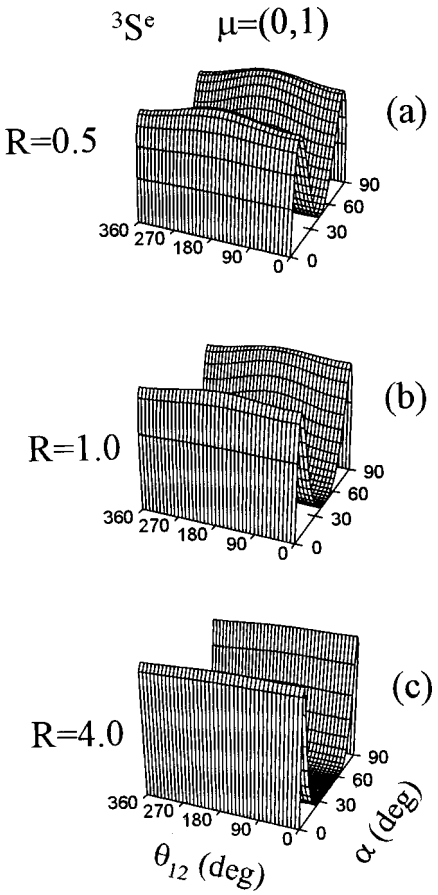

FIG. 6. Three-dimensional surface charge-density $\rho_s(R,\alpha,\theta_{12})$ plots for the $\mu=(0,1)$ channel of symmetry $^3S^e$.

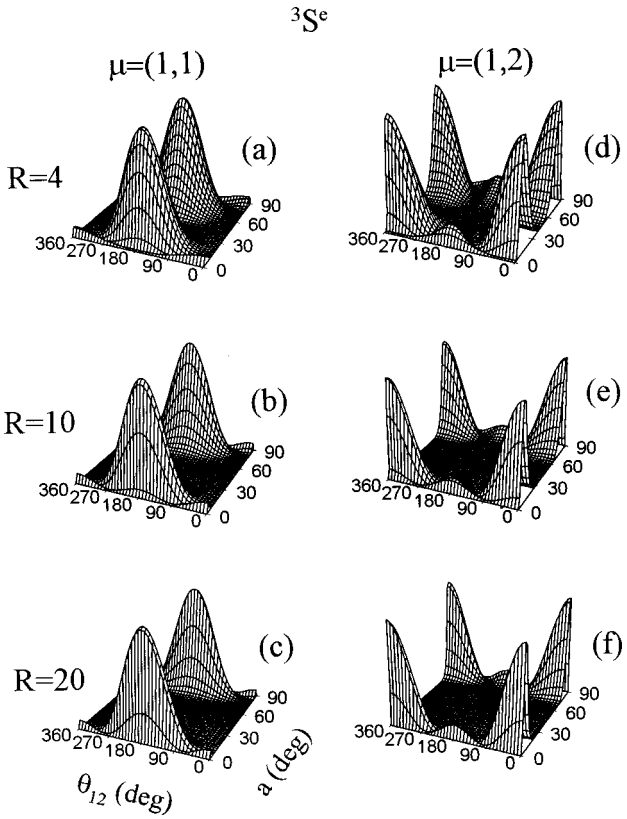

FIG. 7. Three-dimensional surface charge-density $\rho_s(R,\alpha,\theta_{12})$ plots for the $\mu=(1,1)$ and, (1,2) channels of symmetry $^3S^e$.

vicinity of $R=0.25$ and converges to $\epsilon_0=-2$ at large R. The potential well is strong enough to support one bound state, corresponding to the ground state of the D^- center. With this potential curve as the input of Eq. (22), we obtain a ground-state energy -2.262 [marked by a horizontal line in Fig. 2(a)], and -2.239 if the diagonal coupling matrix element $W_{\mu\mu}(R)$ is included. These values compare well with the exact variational result -2.240.[26] Further improvement can be made by considering the couplings of different channels.

In Fig. 3, we present the surface charge-density plots of channel (0, 1) for $R=0.5$, 1.0, and 4.0, to illustrate how the correlation pattern changes as the system evolves from the overcompressed state at small R to the fragmented state at large R. Note that when R is small the kinetic energy term $\Lambda^2/(2R^2)$ is dominant, which can be minimized by smooth distribution of the wave function; when R is large, the Coulomb term $C(\Omega)/R$ is dominant, which can be minimized by concentrating the wave function at the minimum of $C(\Omega)$ and in its vicinity. In Figs. 3(a) and 3(b), where R is small, the surface charge density spreads smoothly over the whole (α,θ_{12}) plane. There is a pronounced peak at $(\alpha,\theta_{12})=(45°,180°)$ in Fig. 3(a), which favors the reduction of the electron-electron Coloumb repulsion. In Fig. 3(c) where R is relatively large, the surface charge density concentrates its distribution in the valleys of the potential surface $C(\Omega)$ shown in Fig. 1. Since a change in θ_{12} amounts to little change in $r_{12}=R[1-\sin(2\alpha)\cos\theta_{12}]^{1/2}$ as $\alpha\sim 0$ or $\alpha\sim 90°$, there is no noticeable θ_{12} dependence of the surface charge density in Fig. 3(c). This quick loss of angular correlation causes the electric dipole moment of the neutral donor, which governs the interaction between the neutral core and the outer electron, to vanish quickly with increase of R. For this reason, the attractive well exhibited in Fig. 2(a) is very narrow.

In Fig. 2(b), there are two channels converging to $\epsilon_1=-\frac{2}{9}\approx -0.222$. Channel (1,1) has an attractive well in the vicinity of $R=4$, which supports one bound state. This is the lowest doubly excited state of the system. It is stable within the adiabatic approximation. Channel (1,2) is entirely repulsive.

The surface charge-density plots for these two channels are displayed in Fig. 4 for $R=4$, 10, and 20. As we proceed from the ground channel (0,1) to higher channels, the channel functions $\Phi_\mu(R,\Omega)$ at each R may exhibit nodal lines which arise from kinematics and characterize different modes of internal motion, like different normal modes of standing waves on a drumhead. Remember that the distribution of the higher channel functions is determined by both the minimization of energy and orthogonality to lower channels. In Figs. 4(a)–4(c), we first notice that the (1,1) channel has most of the charge density in the region $90°<\theta_{12}<270°$, and peaks at $\theta_{12}=180°$; i.e., the two electrons tend to stay on opposite sides of the donor ion. In Fig. 4(a), channel (1,1) minimizes the kinetic energy and electron-electron repulsion by concentrating the charge distribution at

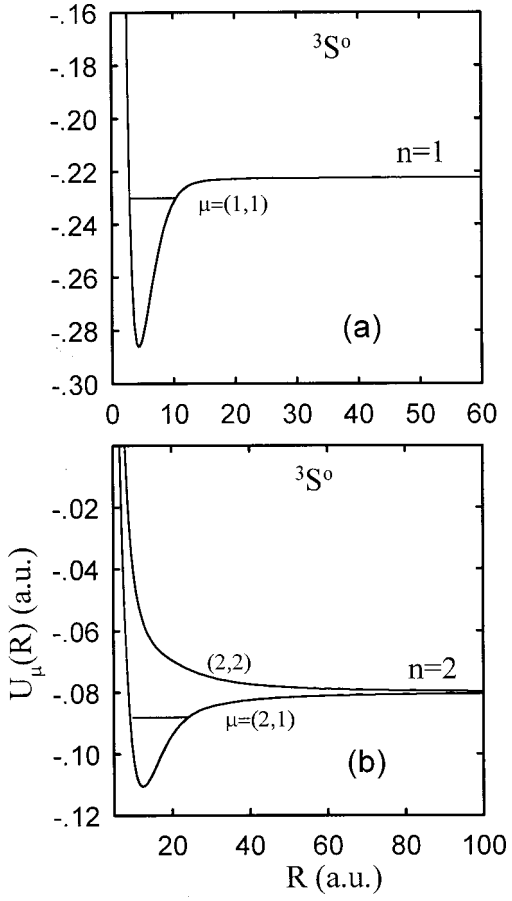

FIG. 8. Potential curves for $^3S^o$ channels converging to the ϵ_n limit: $n=$(a) 1, (b) 2. The horizontal lines mark the bound states supported by the potentials.

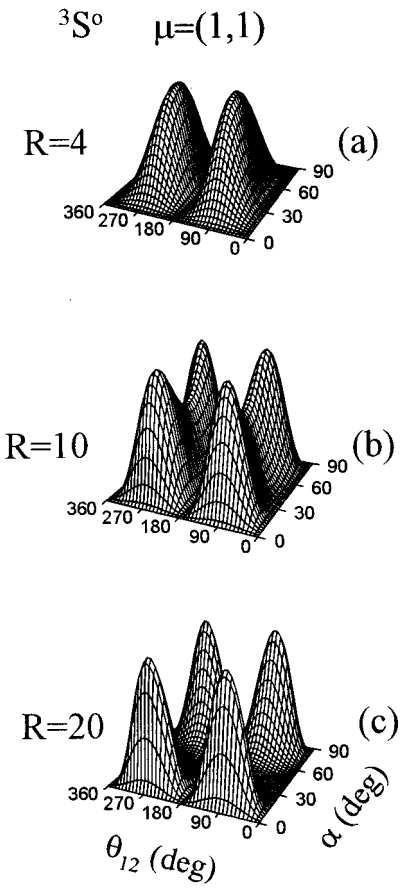

FIG. 9. Three-dimensional surface charge-density $\rho_s(R,\alpha,\theta_{12})$ plots for the $\mu=(1,1)$ channel of symmetry $^3S^o$.

$(\alpha,\theta_{12})=(45°,180°)$ and in its vicinity. As R increases, the charge distribution begins to shift to the $\alpha\approx 0$ and 90° regions and the charge density near $\alpha\approx 45°$ drops as channel (0,1) does. However, unlike in channel (0,1), the angular correlation in channel (1,1) remains almost unchanged. This pertinacious angular correlation results in the slower convergence of the corresponding potential curve to its threshold than channel (0,1) as $R\rightarrow\infty$. Comparing Fig. 3(c) with Fig. 4(a), we notice that the space occupied by channel (1,1) is that unoccupied by channel (0, 1); additionally, there are two less conspicuous nodal lines near $\alpha=0$ and 90°, respectively, in channel (1,1). From these factors, channel (1,1) achieves its orthogonality to channel (0,1).

The surface charge-density plots for channel (1, 2) are displayed in Figs. 4(d)–4(f). We notice that this repulsive channel has most of its charge density in the regions $\theta_{12}<90°$ and $\theta_{12}>270°$; i.e., the two electrons tend to stay on the same side of the donor ion. In Fig. 4(d), where the kinetic energy dominates, the charge density shows a considerable smooth spread over the full (α,θ_{12}) plane with two peaks at $(\alpha,\theta_{12})=(45°,0)$ and (45°,360°), respectively. These are the positions where the two spikes of $C(\Omega)$ are located. Thus the two electrons experience large electron-electron interaction in channel (1,2). These regions are preferable to the central region since they are unoccupied by channels (0, 1) and (1,1). Forcing the distribution of charge density to the central region of the (α,θ_{12}) plane (i.e., forcing the two electrons to opposite sides of the donor ion) would require additional nodal lines in order to achieve orthogonality to channels (0,1) and (1,1). For $R\geqslant 20$, the central region is left unoccupied by channels (0,1) and (1,1), but channel (1,2) does not shift to this region since at these large R values the regions where $\alpha\approx 0$ or 90° are more favorable in order to minimize the Coulomb potential energy. For this reason, the θ_{12} dependence of the charge density remains almost unchanged as R increases.

B. The $^3S^e$ channels

The low-lying potential curves in the $^3S^e$ symmetry are displayed in Fig. 5. They shift their wells to ranges of larger R than their counterparts in the $^1S^e$ symmetry, due to stronger centrifugal barriers. For the (0,1) channel, the potential curve converges to its limit very quickly and the potential well is ambiguous. The other channels are also less attractive (or more repulsive) than their counterparts in the $^1S^e$ symmetry.

The corresponding surface charge-density plots are displayed in Figs. 6 and 7. The channel functions in the $^3S^e$ symmetry, which can be expressed as superpositions of the

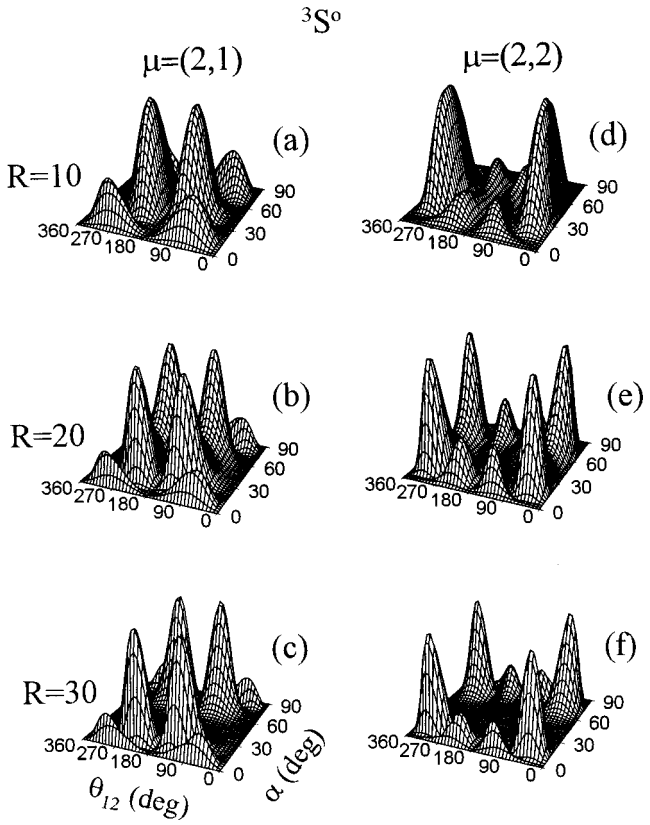

FIG. 10. Three-dimensional surface charge-density $\rho_s(R,\alpha,\theta_{12})$ plots for the $^3S^o$, $\mu=(2,1)$ and (2,2) channels.

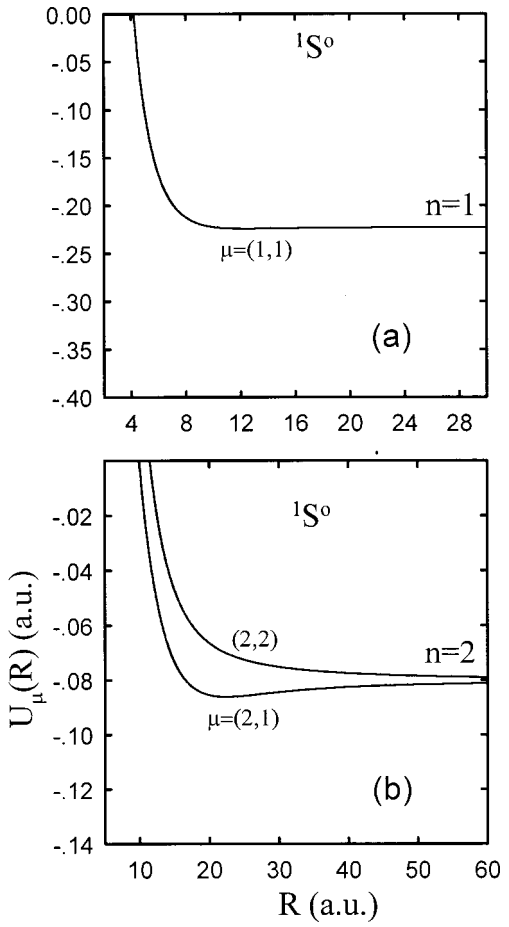

FIG. 11. Potential curves for $^1S^o$ channels converging to the ϵ_n limit: $n=$(a) 1, (b) 2.

basis functions $|n\nu l-\rangle^e$, differ from the channel functions in the $^1S^e$ symmetry by the existence of an inherent nodal line along $\alpha=45°$. Because of this nodal line, the potential curves $U_\mu(R)$ are significantly higher than their counterparts in the $^1S^e$ symmetry in the ranges of small R. A drastic internal motion across the ridge of $C(\Omega)$ is induced. The distribution of charge density is driven away from $\alpha=45°$ and its vicinity. In the ranges of large R where the distributions of charge density shifts to the $\alpha\approx 0$ and 90° regions and the charge density drops to zero near $\alpha=45°$, whether there is a nodal line along $\alpha=45°$ or not makes no difference. Thus the corresponding potential curves in both symmetries tend to coincide. The similarity between the $^1S^e$ and the $^3S^e$ channel functions at large R values is visualized by comparing, for example, Fig. 4(c) with Fig. 7(c), and Fig. 4(f) with Fig. 7(f), etc.

C. The $^3S^o$ channels

The low-lying potential curves for the $^3S^o$ symmetry are presented in Fig. 8. In the $^3S^o$ symmetry, there is no channel converging to ϵ_0. There is one channel converging to ϵ_1, which exhibits a narrow attractive well because the dipole interaction vanishes, like the (0,1) channel of symmetry $^1S^e$. But the physical pictures in the two cases are entirely different: In the (0,1) channel of symmetry $^1S^e$, the dipole interaction vanishes because there is no angular correlation when R is up to a certain value, while in the (1,1) channel of symmetry $^3S^o$ it is because the angular correlation is so strong that the position vectors of the two electrons are maintained on average in vertical directions, as will be shown in the following. There are two channels converging to ϵ_2; channel (2,1) shows an attractive well and supports one bound state and channel (2,2) is entirely repulsive.

The surface charge-density plots for these channels are displayed in Figs. 9 and 10. The channel functions in the $^3S^o$ symmetry, which can be expressed as superpositions of the basis functions $|n\nu l+\rangle^o$, are characterized by the existence of two inherent nodal lines along $\theta_{12}=180°$ and 0 (or $\theta_{12}=360°$), respectively. These nodal lines prohibit the two electrons from staying on the same side or on opposite sides of the donor ion to form a collinear structure. In channel (1,1), the two electrons tend to stay in a configuration with $\theta_{12}=90°$ (or $\theta_{12}=270°$) and $r_1=r_2$ (i.e., $\alpha=45°$) when R is small [see Fig. 9(a)]. As R increases, the charge density shifts to the regions $\alpha\approx 0$ and 90°, but the influence of the inherent nodal lines and thus the pattern of angular correlation is maintained [see Figs. 9(b) and 9(c)].

In Figs. 10(a)–10(c), where the surface charge-density plots for channel (2,1) are displayed, the charge density is distributed mostly in the regions $90°<\theta_{12}<180°$ and $180°<\theta_{12}<270°$, such that $\cos\langle\theta_{12}\rangle_\mu<0$, i.e., the dipole interaction is attractive in the channel, although the two electrons

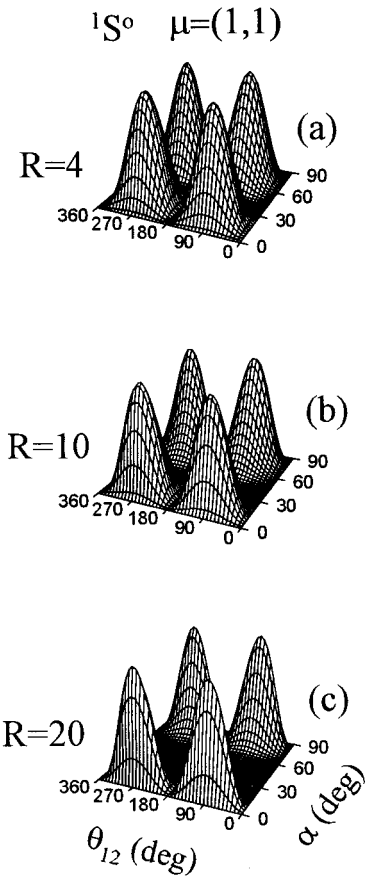

FIG. 12. Three-dimensional surface charge-density $\rho_s(R,\alpha,\theta_{12})$ plots for the $\mu=(1,1)$ channel of symmetry $^1S^o$.

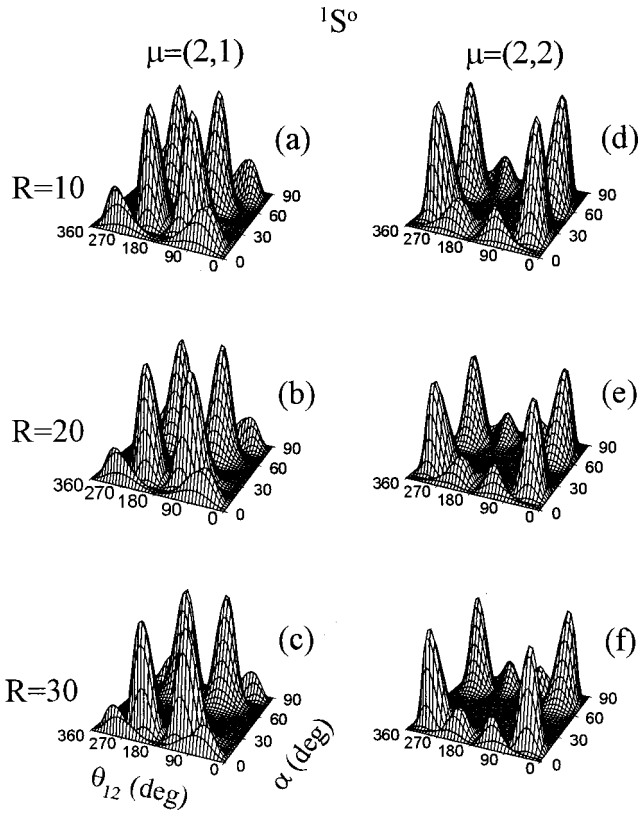

FIG. 13. Three-dimensional surface charge-density $\rho_s(R,\alpha,\theta_{12})$ plots for the $\mu=(2,1)$ and (2,2) channels of symmetry $^1S^o$.

and the donor are prohibited from forming a collinear structure. In addition, there are two additional nodal lines along $\alpha=$const, which shift their locations toward $\alpha=0$ and 90°, respectively, as R increases.

In Figs. 10(d)–10(f), where the surface charge-density plots for channel (2,2) are displayed, the charge density is distributed mostly in the regions $0°<\theta_{12}<90°$ and $270°<\theta_{12}<360°$. A repulsive dipole interaction is expected in the channel. There are two additional nodal lines along $\theta_{12}=$const, the locations of which remain unchanged as R increases.

D. The $^1S^o$ channels

The low-lying potential curves for the $^1S^o$ symmetry are presented in Fig. 11. As in the $^3S^o$ symmetry, there is no channel converging to ϵ_0. There is one channel converging to ϵ_1, which is entirely repulsive and converges quickly to its threshold. There are two channels converging to ϵ_2. The attractive potential well exhibited by channel (2,1) is ambiguous. Channel (2,2) is entirely repulsive. Comparing Fig. 11 with Figs. 2, 5, and 8, one will find that channels in the $^1S^o$ symmetry are higher than their counterparts in any other symmetries discussed above.

The corresponding surface charge-density plots are displayed in Figs. 12 and 13. The channel functions in this symmetry can be expressed as superpositions of the basis functions $|n\nu l-\rangle^o$ and have all three inherent nodal lines we have found above, i.e., the nodal lines along $\alpha=45°$, $\theta_{12}=0$ (or 360°), and $\theta_{12}=180°$. The coexistence of these nodal lines, especially the ones along $\alpha=45°$ and $\theta_{12}=180°$, leaves little space for the minimization of energy. In the ground channel $\mu=(1,1)$, where the inherent nodal lines are the only nodal lines of the channel function (see Fig. 12), the charge density is concentrated into four identical peaks in order to avoid the nodal lines. Evidently, this channel has $\cos\langle\theta_{12}\rangle_\mu=0$ in all ranges of R and the dipole interaction vanishes. In the (2, 1) channel [see Figs. 13(a)–13(c)], there are two additional nodal lines associated with the variation of α. The distribution of charge density is mostly in the regions $90°<\theta_{12}<180°$ and $180°<\theta_{12}<270°$ such that $\cos\langle\theta_{12}\rangle_\mu<0$, i.e., the dipole interaction is attractive. In the repulsive (2, 2) channel [see Figs. 13(d)–13(f)], the number of nodal lines is the same as in channel (2, 1), but the charge density shifts mostly to the regions $0°<\theta_{12}<90°$ and $270°<\theta_{12}<360°$, such that the dipole interaction is repulsive. In the ranges of large R, the charge distributions for the $^1S^o$ channels are similar to their counterparts in the $^3S^o$ symmetry, which can be seen by comparing, for example, Fig. 9(c) with Fig. 12(c), etc.

IV. SUMMARY

In this paper, we have demonstrated the adiabatic potential curves and corresponding correlation patterns for two electrons in the low-lying $L=0$ states. Four different sym-

metries have been covered. The $^{1,3}S^e$ symmetries have their counterparts in three dimensions,[13] but the $^{1,3}S^o$ symmetries do not. Our main findings can be summarized as follows.

(a) The correlation pattern of a channel is determined by three competing factors: the minimization of energy, the orthogonality to the lower channels, and the symmetry constraints. The minimization of energy is achieved by smooth spread of the charge density when R is small and by gradual concentration of the charge density in the potential valleys as R increases. There are two different ways to achieve orthogonality to lower channels, i.e., by occupying areas unoccupied by the lower channels or by introducing more nodal lines in the channel function. The role of symmetry is embodied by the existence of certain inherent nodal lines in the channel functions.

(b) The angular correlations in the ground channels of the $^{1,3}S^e$ symmetries are weak and tend to vanish quickly as R increases, while the angular correlations in the doubly excited channels are strong and, once established at small R, the patterns remain nearly unchanged as R increases.

(c) Whether the channels in a symmetry are high or low lying in comparison with their counterparts in other symmetries is determined by the number of inherent nodal lines in the channel functions. Among the four symmetries we have studied, the channel functions in the $^1S^e$ symmetry have no inherent nodal lines, while the channel functions in the $^1S^o$ symmetry have the biggest number of inherent nodal lines.

(d) There is a connection between the features of a potential curve and the corresponding pattern of angular correlation. If the two electrons are maintained at small angles, $U_\mu(R)$ exhibits a long repulsive tail, and no attractive potential well is expected. If the two electrons are maintained at large angles, $U_\mu(R)$ exhibits a potential well with a long attractive tail. If there is no angular correlation or the position vectors of the two electron are maintained in vertical directions, $U_\mu(R)$ is flat over a wide range of R; whether an attractive well is then exhibited or not depends on the number of nodal lines in the channel function.

Although we have confined our study to four symmetries with $L=0$, these do exhaust all possible combinations of inherent nodal lines. Therefore, any $L\neq 0$ state must have exactly the same inherent nodal lines as one of the four symmetries studied here and have similar patterns of correlation. However, in the case of $L\neq 0$, there is the additional effect of collective rotation, which tends to maintain the system in a collinear structure. This will be discussed elsewhere.

ACKNOWLEDGMENTS

This work was supported by the National Natural Science Foundation of China, Grant No. 19875018, and also in part by the Natural Science Foundation of Guangdong Province and the Natural Science Foundation of Guangzhou City, P. R. China.

*Email address: phwyruan@scut.edu.cn

[1] S. Huant, S. P. Najda, and B. Etienne, Phys. Rev. Lett. **65**, 1489 (1990).
[2] T. Pang and S. G. Louie, Phys. Rev. Lett. **65**, 1635 (1990).
[3] D. M. Larsen and S. Y. McCann, Phys. Rev. B **45**, 3485 (1992).
[4] A. B. Dzyubenko, Phys. Lett. A **165**, 357 (1992).
[5] A. H. MacDonald, Solid State Commun. **84**, 109 (1992).
[6] J. M. Shi, F. M. Peeters, and J. U. Devreese, Phys. Rev. B **51**, 7714 (1995).
[7] J. L. Zhu and S. Xu, J. Phys.: Condens. Matter **6**, L299 (1994).
[8] H. L. Fox and D. M. Larsen, Phys. Rev. B **51**, 10 709 (1995).
[9] C. Riva, V. A. Schweigert, and F. M. Peeters, Phys. Rev. B **57**, 15 392 (1998).
[10] W. F. Xie, J. Phys.: Condens. Matter **12**, 3849 (2000).
[11] W. Y. Ruan, K. S. Chan, H. P. Ho, R. Q. Zhang, and E. Y. B. Pun, Phys. Rev. B **60**, 5714 (1999).
[12] J. H. Macek, J. Phys. B **1**, 831 (1968).
[13] C. D. Lin, Phys. Rep. **257**, 2 (1995), and references therein.
[14] H. Essen, Int. J. Quantum Chem. **12**, 721 (1977).
[15] D. M. Bishop and R. W. Wetmore, Mol. Phys. **26**, 145 (1973).
[16] W. Kolos and L. Wolniewicz, J. Chem. Phys. **41**, 3663 (1964).
[17] C. Schwartz, Phys. Rev. **124**, 1468 (1961).
[18] C. D. Lin, Phys. Rev. A **14**, 30 (1976).
[19] A. S. Jensen, E. Garrido, and D. V. Federov, Few-Body Syst. **22**, 1931 (1997).
[20] C. D. Lin and J. H. Macek, Phys. Rev. A **29**, 2317 (1984).
[21] C. D. Lin and X. H. Liu, Phys. Rev. A **37**, 2749 (1988).
[22] W. Y. Ruan, K. S. Chan, and E. Y. B. Pun, J. Phys.: Condens. Matter **12**, 7905 (2000).
[23] J. J. De Groote, A. S. dos Santos, M. Misili, and J. E. Hornos, Phys. Rev. B **58**, 10 383 (1998).
[24] C. H. Greene, Phys. Rev. A **26**, 2974 (1982).
[25] J. Botero and C. H. Greene, Phys. Rev. A **32**, 1249 (1985).
[26] W. Y. Ruan *et al.* (unpublished).